Contrib Mineral Petrol (2002) 143: 254–261
DOI 10.1007/s00410-001-0339-0

Frank N. Schäfer · Stephen F. Foley

The effect of crystal orientation on the wetting behaviour of silicate melts on the surfaces of spinel peridotite minerals

Received: 29 May 2001 / Accepted: 20 November 2001 / Published online: 26 January 2002

Abstract The effect of crystal anisotropy on wetting angles of equilibrium silicate melts on crystal faces of spinel, diopside, enstatite and olivine has been determined experimentally by the sessile melt drop technique. The anisotropy, $\tilde{A}\gamma_{SL}$, of solid-liquid interfacial energies (γ_{SL}(max)–γ_{SL}(min)) can be related to the wetting angles, ψ, by $\tilde{A}\gamma_{SL} \propto |\cos\psi(\max) - \cos\psi(\min)| = Pw_{(\tilde{A}\gamma_{SL})}$. Normalising to the smallest wetting angle gives values of Pw for diopside = 0.0728, olivine = 0.0574, orthopyroxene = 0.0152, and spinel = 0.0075. Crystal anisotropy influences grain-scale morphology of small-degree partial melts, permeability and the melt connectivity threshold, ϕ_C. Results show that, at sufficient melt fractions, diopside should increase permeability in a peridotitic matrix, whereas enstatite should lower it. Despite its low anisotropy, spinel contributes positively to permeability and ϕ_C because of its high surface energies. These results suggest that harzburgitic mineral matrices typical of the subcratonic mantle should impede the movement of low-degree partial melts, whereas melts should flow more easily through spinel lherzolites.

Introduction

The composition, extractability and migration of partial melts in the upper mantle depend largely on the degree of melting needed to achieve an interconnected melt network. This critical melt fraction depends in turn on the morphology of the melt phase, meaning the degree to which channels along grain boundaries, melt pockets and films make up the total melt fraction (e.g. Bulau and Waff 1979; Laporte and Watson 1995; Drury and Fitz-Gerald 1996; Faul 1997; Cmiral et al. 1998). In general, the melt morphology is a function of the interfacial energies between the melt and individual mineral grains (e.g. Waff and Bulau 1979; Bussod and Christie 1991), and these interfacial energies have mostly been investigated by determination of dihedral angles of melts in mineral matrices (Bulau and Waff 1979; Watson et al. 1990).

However, the anisotropy of mineral-melt interfacial energy, although potentially important in determining melt pathways in both deformed and undeformed rocks, has received relatively little attention, particularly for mantle rocks. In this study, the variation in mineral-melt interfacial energy for different crystal faces of the same mineral, and its influence on melt morphology with regard to permeability and the connectivity threshold, ϕ_C, are investigated experimentally by the sessile melt drop technique. Diopside, enstatite, olivine and spinel were chosen as the main constituents of lithospheric upper mantle peridotites at depths corresponding to the spinel lherzolite field where most primary basaltic melts are generated.

Melt distribution in anisotropic systems

Crystal structural considerations predict that in a solid polycrystalline system the grain boundaries where three grains meet at triple junctions present the paths of easiest passage for melt migration. This is caused by the comparatively weak bonding and occurrence of open spaces at these interfaces due to differences in the structure and orientation of juxtaposed grains. However, the question of whether or not a melt can move freely between grains depends on the volume fraction and wetting properties of that melt (e.g. Bulau and Waff

F.N. Schäfer (✉)
Mineralogisch-Petrologisches Institut,
Universität Göttingen, Goldschmidtstr. 1,
37077 Göttingen, Germany
E-mail: fschaef2@gwdg.de

S.F. Foley (✉)
Institut für Geologische Wissenschaften,
Universität Greifswald, F-L-Jahnstrasse 17a,
17487 Greifswald, Germany
E-mail: sfoley@uni-greifswald.de

Editorial responsibility: J. Hoefs

1979; Nakano and Fujii 1989), of which the latter can be expressed in terms of the interfacial energy between the mineral grain and the melt (γ_{SL}) relative to the interfacial energy between the mineral grains themselves (γ_{SS}). For adjacent mineral grains different values of γ_{SS} depend on the extent of their crystallographic misorientations, but only the crystallographic orientation of the wetted mineral face is decisive for variation of γ_{SL} because the melt can be considered as an isotropic medium. Variation of the mineral-melt interfacial energy, γ_{SL}, is therefore principally the result of crystal anisotropy.

Assuming that melt fraction and wetting conditions allow the formation of an interconnected melt network, the interfaces between minerals and melt in an isotropic mineral matrix would be curved to minimise the total mineral-melt interfacial energy of that system. However, in the case of natural undeformed peridotites the anisotropy of the approximately randomly orientated crystals will lead to a mixture of curved and flat faces (Waff and Faul 1992; Laporte and Watson 1995; Cmiral et al. 1998). Crystal faces which retain a flat shape in contact with melt because of their minimum surface energy were termed flat faces (F-faces) by Waff and Faul (1992). F-faces are important for permeability because of the increased cross-sectional area of any melt channels they abut against (Fig. 1). The tendency of mineral grains to develop F-faces along melt-filled channels depends mainly on the magnitude of the anisotropy of solid-liquid interfacial energies γ_{SL} (Laporte and Provost 1993; Rignault et al. 1996; Holness 1997; Cmiral et al. 1998). This anisotropy, expressed as $\tilde{A}\gamma_{SL} = \gamma_{SL}(\max) - \gamma_{SL}(\min)$, thus exerts a major control on the morphology of the melt phase and on the connectivity threshold (ϕ_C), which is the minimum melt fraction needed to form an interconnected melt network.

In isotropic mineral matrices where the interfaces of melt pockets are convex inwards, interconnectivity can be reached at extremely low melt fractions provided that the dihedral angle is suitably low (McKenzie 1984). By contrast, anisotropy of crystals leads to a higher connectivity threshold due to the bounding of melt pockets by F-faces, and consequently to larger volumes of the melt pockets (Laporte and Watson 1995).

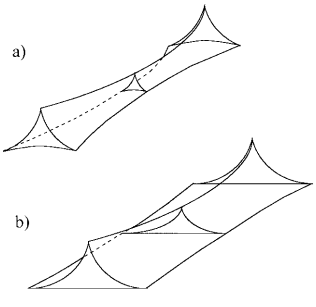

Fig. 1a, b. Depiction of a melt channel along a grain triple junction **a** with curved interfaces, and **b** with one flat face boundary. The cross-sectional area in **b** is larger than in **a** (after Waff and Faul 1992)

Relation of $\tilde{A}\gamma_{SL}$ to wetting angles

The aim of this study is to obtain information about the anisotropy of mineral-melt interfacial energies $\tilde{A}\gamma_{SL}$ for spinel peridotite minerals in order to estimate the melt morphology in peridotitic systems. For this purpose wetting angles of silicate melt drops were experimentally produced on crystallographically defined crystal surfaces. Here, the relation between measured wetting angles and $\tilde{A}\gamma_{SL}$ is briefly explained.

The wetting angle ψ of a melt drop on a flat mineral surface at equilibrium is a function of all three interfacial energies (e.g. Bischof and Possart 1983; Wanamaker and Kohlstedt 1991) and is described by the equation of Young:

$$\cos\psi = \frac{\gamma_{SV} - \gamma_{SL}}{\gamma_{LV}} \quad (1)$$

where γ_{SL}, γ_{SV} and γ_{LV} are the solid-liquid, solid-vapour and liquid-vapour interfacial energies respectively (Fig. 2). It is not possible to quantify values for one of these interfacial energies by means of the wetting angle alone. However, in case of homogenous melt and gas phases (i.e. γ_{LV} has a constant value), the variation of wetting angles between crystal faces with different crystallographic orientation depends solely on the difference of $\gamma_{SV}-\gamma_{SL}$. Thus, these two interfacial energies are directly proportional to the wetting angles on different faces of a given mineral, and this proportionality is independent of γ_{LV}.

Interfacial energies are commonly represented by vectors acting on the triple junction where melt, gas and solid come together as shown in Fig. 2. These vectors can be considered as tensions pulling at the triple junction which result from adhesive forces of the three phases which act at equilibrium in a perpendicular direction to the interfaces. The crystal face then serves as a rigid plane on which the deformable melt drop is forced by these tensions to move its boundaries (triple junction) until an equilibrium shape is achieved. Figure 3 is a schematic representation of these forces acting along the interfaces in case of an increase in the crystal surface energy (γ solid-vacuum) a by δa together with a decreasing value of the force b_1 acting in the opposite direction. This force is caused by the melt particles and lowers a by b_1 so that

$$\gamma_{SL} = a_{SL} - b_1 \text{ and } \gamma_{SV} = a_{SV} \quad (2)$$

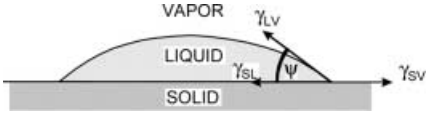

Fig. 2. Schematic diagram of a melt drop on a crystal surface. The relative magnitudes of the three interfacial energies acting at the triple junction of all three phases determine the wetting angle ψ (from Wanamaker and Kohlstedt 1991)

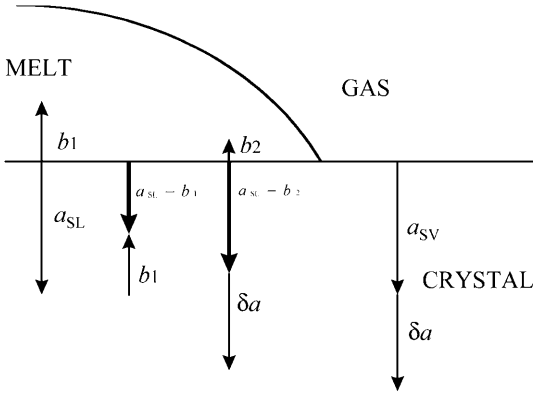

Fig. 3. Schematic diagram of force vectors involved in control of droplet shape by interfacial energies (see text for explanation)

when neglecting the force component exerted by the gas phase.

With increasing surface energy of the crystal face the value of b_1 decreases to b_2, as indicated by the results from Wanamaker and Kohlstedt (1991), entailing a decreasing difference between γ_{SV2} and γ_{SL2} (where 1 and 2 stand for cases 1 and 2)

$$a\mathrm{SV} - (\mathrm{aSL} - b_1) = \gamma_{SV1} - \gamma_{SL1} \quad (3)$$

$$(a_{SV} \pm \delta a) - (a_{SL} \pm \delta a - b_2) = \gamma_{SV2} - \gamma_{SL2} \quad (4)$$

which means that

$$\gamma_{SV2} - \gamma_{SL2} < \gamma_{SV1} - \gamma_{SL1} \quad (5)$$

Because of $\alpha_{SV} = \alpha_{SL}$ and therefore $b_1 = \gamma_{SV1} - \gamma_{SL1}$, and $b_2 = \gamma_{SV2} - \gamma_{SL2}$, it follows that a change in value depends on $\delta b = b_1 - b_2$. With constant melt composition, a change of δb (variation of γ_{SL}) is linked to a change in δa (variation of γ_{SV}), and can be expressed by

$$\gamma_{SL2} - \gamma_{SL1} = \delta b + \delta a \quad (6)$$

These two quantities also determine a change in the wetting angle:

$$(\gamma_{SV2} - \gamma_{SV1}) - (\gamma_{SL2} - \gamma_{SL1}) = \cos\psi_2 \cdot \gamma_{LV} - \cos\psi_1 \cdot \gamma_{LV} \quad (7)$$

Considering constant compositions for melt and gas phases, γ_{LV} is a constant, and so Eq. (7) can be rearranged and simplified to

$$(\gamma_{SL2} - \gamma_{SL1}) = (\gamma_{SV2} - \gamma_{SV1}) - \cos\psi_2 - \cos\psi_1 \quad (8)$$

Substituting Eqs. (1), (2) and (3), Eq. (8) becomes

$$(a - b_2 \pm \delta a) - (a - b_1) = (a \pm \delta a - a) - (\cos\psi_2 - \cos\psi_1) \quad (9)$$

Removing the brackets leads to

$$b_1 - b_2 = \delta b = \cos\psi_1 - \cos\psi_2 \quad (10)$$

Comparing Eq. (6) with Eq. (10), it becomes clear that

$$|b_1 - b_2| \propto |\gamma_{SL2} - \gamma_{SL1}|$$

and therefore

$$|\gamma_{SL2} - \gamma_{SL1}| \propto |\cos\psi_1 - \cos\psi_2| \quad (11)$$

This proportionality emphasises the dependence of the wetting angles on the relative magnitude of the interfacial energies γ_{SL} which is equivalent to

$$\tilde{\mathrm{A}}\gamma_{SL} \propto |\cos\psi(\max) - \cos\psi(\min)|$$

This means that wetting-angle values will be greater for crystal faces with higher surface energies for a given mineral.

Experimental procedure

We employed the sessile melt drop technique previously used by Wanamaker and Kohlstedt (1991) in their study of olivine. This technique consists of measurement of the wetting angle ψ, which is the angle between the surface of the drop and the crystal face at the point of solid-liquid-vapour intersection when the drop is viewed in cross section (Fig. 2). Crystal substrates (Table 1) were large single crystals chosen to represent constituents of

Table 1. Compositions and localities of minerals used as mineral substrates in melt drop experiments

Mineral	Spinel 4.60 ct	Spinel 4.63 ct	Spinel 5.21 ct	Enstatite	Diopside	Forsterite
Provenance	**Sri Lanka**, Radnapura Valley	**Sri Lanka**, Radnapura Valley	**Sri Lanka**, Radnapura Valley	**Lepontine Alpes**, Semione (Biasca)	**East Siberia**, Inagli	**Arizona (USA)**, San Carlos
Composition (wt%)						
SiO_2	0.03	0.02	0.04	57.64	56.09	41.63
TiO_2	0.01	0.04	0.02	0.03	0.07	0.01
Al_2O_3	70.11	70.81	70.51	0.04	0.20	0.03
Cr_2O_3	0.01	0.10	0.01	0.05	0.56	0.04
FeO	1.24	0.67	0.91	8.90	1.07	8.56
MnO	0.02	0.05	0.03	0.10	0.05	0.13
MgO	27.33	27.61	27.69	33.65	17.88	51.33
CaO	0.01	0.01	0.00	0.07	25.14	0.10
Na_2O	0.00	0.00	0.01	0.01	0.32	0.02
K_2O	0.00	0.00	0.01	0.01	0.01	0.01
Sum	98.77	99.32	99.20	100.48	101.39	101.85

Table 2. Composition of synthetic melts used in melt drop experiments, listed by the mineral with which they were used in combination

Mineral	Composition of corresponding melt mixture (wt%)									Reference
	SiO_2	TiO_2	Al_2O_3	Cr_2O_3	FeO	MgO	CaO	Na_2O	K_2O	
Spinel	51.00	–	23.50	–	–	25.50	–	–	–	Levin et al. (1974)
Enstatite	51.45	2.50	14.36	0.44	5.50	11.06	11.49	2.13	0.56	Cmiral et al. (1998)
Diopside	61.60	–	–	–	–	8.80	29.60	–	–	Levin et al. (1974)
Forsterite	51.45	2.50	14.36	0.44	5.50	11.06	11.49	2.13	0.56	Cmiral et al. (1998)

Table 3. Combination of vectors ($\vec{x}$, $\vec{y}$, $\vec{z}$) representing the Cartesian co-ordinates of the crystal axes in a reference frame which are necessary to get the vectors (co-ordinates) of the desired crystal faces (X, Y, Z). The components of vector Z which is needed to define the desired planes are always given by the origin of the co-ordinate system (0, 0, 0). For diopside a monoclinic angle $\beta = 105.9°$ (Bruno et al. 1982) was used

Faces	X	Y	Z
(111)	$\vec{x} - \vec{z}$	$\vec{y} - \vec{z}$	0, 0, 0
(110)	$x - z - y$	$y - z - x$	0, 0, 0
(101)	$\vec{x} - \vec{y} - \vec{z}$	$\vec{z} - \vec{y} - \vec{x}$	0, 0, 0
(011)	$\vec{z} - \vec{x} - \vec{y}$	$\vec{y} - \vec{x} - \vec{z}$	0, 0, 0
(210)	$\vec{x} - \vec{z} - \vec{y} - 1/2\,\vec{x}$	$\vec{y} - \vec{z} - \vec{x} + 1/2\,\vec{x}$	0, 0, 0
Diopside (001)	$\cos(90 - \beta)\vec{x} - \sin(90 - \beta)\vec{z}$	$\vec{y}$	0, 0, 0
Diopside (110)	$(\cos(90 - \beta)\vec{x}) - \vec{z} - \vec{y}$	$\vec{y} - \vec{z} - (\cos(90 - \beta)\vec{x})$	0, 0, 0

spinel peridotites in the uppermost mantle. Melts for experiments with orthopyroxene and olivine were a synthetic basalt mixture after Cmiral et al. (1998), whereas for diopside and spinel synthetic glasses were chosen to be equilibrium compositions on the basis of the appropriate ternary phase diagrams from Levin et al. (1974). Melt compositions are listed in Table 2.

Experiments were conducted on surfaces of at least 100 mm^2 with defined crystallographic orientation. These samples were prepared by first setting the minerals in cubes of epoxy resin and then polishing, using several polishing steps and a final polish with colloidal silica to achieve a crystal surface with minimal damage. The cube edges served as a reference frame for subsequent orientation by analysis using electron back-scattered patterns (EBSP; Neumann 1996), performed with a Leo 1530 Gemini scanning electron microscope with a Nordif detector. The best patterns were produced with an accelerating voltage of 20 kV and a nominal beam current of 10 nA. Indexing of the EBSPs was carried out with the computer program Channel+ which resulted in three Euler angles (Bunge 1985) which relate both co-ordinate systems of the reference frame and the crystal lattice by a sequence of rotations. The Euler angles were inserted into an orientation matrix (see Faul and Fitz-Gerald 1999, and references therein) to obtain the Cartesian co-ordinates of the crystal axes represented by three vector components for each axis. The co-ordinates (vectors) for desired crystal faces which were different from the principal faces (100), (010) and (001) were obtained by relating their vector components to the respective Cartesian co-ordinates by a combination of vectors, as shown in Table 3. In the case of diopside a monoclinic angle of $\beta = 105.9°$ (Bruno et al. 1982) was taken into consideration. Then, by means of the analytical geometry program GeoSekII (freeware under http://schulphysik.de/prog3.html) and trigonometric calculations, the intersection lines of the desired crystal faces with the reference cube were determined. Finally, the crystal slabs were cut out of the resin cubes parallel to the desired lattice planes, and repolished (see above).

Melt drop experiments were performed in a high-temperature furnace under a controlled H_2–CO_2 atmosphere at an oxygen fugacity between the iron-wustite and magnetite-wustite buffers. The experimental temperatures were controlled by a $Pt_{94}Rh_6$–$Pt_{70}Rh_{30}$ thermocouple and are listed for each experiment in Table 4 together with the oxygen fugacities. For the determination of fugacities a solid electrolyte oxygen sensor from Ceramic Oxide Fabricators Pty. Ltd. (model: $SIRO_2$ C700+) with a platinum-coated ZrO_2-based pellet was used. The sample consisted of shards of glass placed on a thin mineral slab. These materials were transported with a horizontal guiding device directly into the hotspot of the furnace in order to eliminate vibrations and optimise the retention of an equilibrium drop shape during quenching. After 10–15 min experimental duration, samples were quenched at a rate of $\gg$1,000 °C/min by rapid retraction of the guiding device from the furnace.

Melt drop analysis

Determination of the wetting angles of the quenched melt drops was performed by optical interference microscopy, viewing from above with monochromatic light of wavelengths λ between 436 and 600 nm. This method generates interference fringes on the surface of the melt drops, of which each Ni–th fringe at horizontal distance x from the drop rim represents a height d of the drop surface above the mineral surface. The wetting angle ψ was calculated using $d = (2Ni - 1)\frac{\lambda}{4n}$ and the trigono-

metric relation $\tan\psi = \frac{(2Ni-1)\cdot\lambda}{4\cdot n\cdot x}$, where n is the refractive index of the glass drop. The refractive indices were calculated following Scholze (1988). Reliability of the data obtained was checked by cutting representative samples through the centre of drops perpendicular to the crystal surface/melt interface and measuring the angle directly. This approach was particularly useful for spinel, which exhibited high contact angles difficult to measure accurately by interference microscopy alone. Direct measurements on the cross-sectioned melt drops agree well with the values obtained by interference microscopy.

The measured ψ values are averages of multiple measurements made on several melt drops on a single crystal surface. The measurements are very reproducible with only minor errors (Table 5) due to a loss of precision in counting interference fringes (*Ni*) at high magnification (500×). This high magnification was needed to distinguish single fringes for wetting angles of more than ca. 10°. This corresponds to an error of ±2° for wetting angles in this range.

Following Wanamaker and Kohlstedt (1991), only the first three to eight fringes closest to the rim were used for wetting-angle determinations to minimise the error due to the curvature of the drop surface. In addition, cross-sectioned and polished crystal-melt interfaces were investigated by means of a Jeol JXA-8900R electron microprobe (Geochemical Institute, University Göttingen) to check for possible chemical reaction. Experiments with enstatite were the only ones which did not show very sharp chemical transitions across which no variation of melt or mineral compositions could be detected. Microscopic observations confirmed that, except for orthopyroxene, crystal-melt interfaces remained flat, so that the fundamental force balance of Young's equation (Eq. 1) finds unrestricted application to our results.

Results

The wetting angles measured from the melt drop experiments as a function of crystal orientation are given in Table 5. The wetting angles in the present study showed a clear dependence on the crystallographic orientation of the crystal faces for each mineral, in agreement with the results for olivine of Wanamaker and Kohlstedt (1991). The anisotropy was smallest for spinel, as expected for an isometric mineral.

It should be noted that the values for orthopyroxene have the largest error due to chemical reaction which resulted in pitting of the mineral surface. However, as pitting occurred equally on all crystal faces, the ratio of measured angles is probably little affected, and so the position of orthopyroxene in the order of anisotropy is considered accurate. As mentioned above, the other minerals showed no sign of chemical reaction at the crystal/glass interface, neither in deviation of contact angle nor in chemical composition, as checked by electron microprobe.

To meaningfully compare the anisotropy of the minerals, we relate the measured wetting angles as a function of crystallographic orientation to the interfacial energies by means of a proportionality term (*Pw*), which can be calculated from

$$Pw_{(\tilde{\mathbf{A}}\gamma_{SL})} = |\cos\psi(\max) - \cos\psi(\min)| \propto \tilde{\mathbf{A}}\gamma_{SL}$$

Pw is proportional to $\tilde{\mathbf{A}}\gamma_{SL}$ as derived above, and can vary between a maximum value of 2 and a minimum of zero, or for melt/crystal interfaces to a range between 0 (minimum anistropy or isotropic conditions) and 1 (maximum anisotropy). Values were compared by normalising the smallest wetting angle of a mineral to $\cos 0 = 1$, and then inserting the difference to the maximum angle as ψ(max) into the above equation. As an

Table 4. Temperatures at which the experiments were performed and corresponding oxygen fugacities

	Spinel	Enstatite	Diopside	Forsterite
T (°C)	1,395	1,207	1,342	1,207
fO_2 (bar)	1.2×10^{-8}	6.9×10^{-11}	1.6×10^{-9}	6.9×10^{-11}

Table 5. Wetting angles ψ measured for various crystal surfaces by interference microscopy and usage of profile cuts through melt drops (spinel). Inserting maximum variation of counted numbers for interference fringes (*Ni*) at distance x from the drop rim into the trigonometric equation (see text) gives the approximate error ranges shown in parentheses. Error for spinel results from uncertainty in direct measurement on cross sections of droplets

ψ	Spinel	Enstatite[a]	Diopside	Forsterite
(100)	35° (±1°)	15° (±2°)	24° (±2°)	22° (±2°)
(010)	35° (±1°)	6° (±0.5°)	2° (±0.1°)	2.5° (±0.1°)
(001)	35° (±1°)	16° (±2°)	8° (±1°)	3.8° (±0.2°)
(110)	42° (±1°)	–	14° (±2°)	–
(210)	–	14° (±2°)	–	–
(111)	37° (±1°)	–	–	–

[a]Angles for enstatite may be overestimated due to pitting of the mineral surface by chemical reaction with the melt

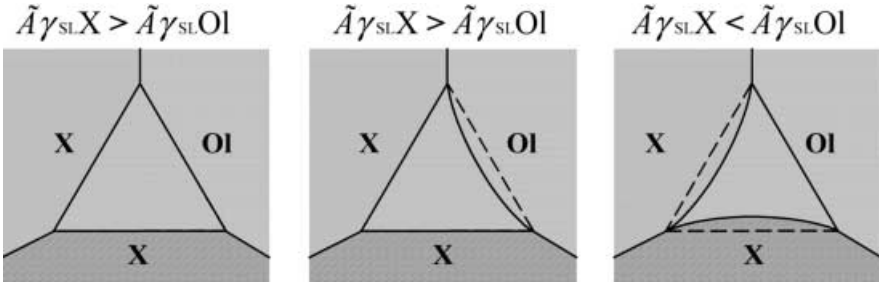

Fig. 4. Schematic diagram of the cross-sectional area of melt channels at triple junctions to emphasise the dependence of their form on relative anisotropy $\tilde{A}\gamma_{SL}$ of the adjoining mineral grains. With more minerals having $\tilde{A}\gamma_{SL} > \tilde{A}\gamma_{SL}Ol$ the likelihood of developing F-faces rises and the pore volume increases. This is also true for channels or pools bounded by more than three grains

example, the following calculation is obtained for spinel: $42° - 35° = 7° \rightarrow Pw_{(\tilde{A}\gamma_{SL})} = |\cos 7 - \cos 0| = 0.0075$.

The four investigated minerals show distinct differences in their degree of anisotropy, ranging from spinel ($Pw = 0.0075$) with the lowest value through enstatite ($Pw = 0.0152$) and forsterite ($Pw = 0.0574$) to diopside ($Pw = 0.0728$).

Discussion

Melt connectivity and permeability in spinel peridotites

A principal requirement for melt segregation and extraction under upper mantle conditions is the mobility of partial melts at the grain scale. This in turn depends on the distribution and morphology of the melt within the grain matrix (Faul 1997). As soon as an interconnected network of the melt phase is achieved (denoted here as the connectivity threshold, ϕ_C), the matrix becomes permeable. The melt fraction needed to achieve connectivity is controversial and lies somewhere in the range <1 to a few vol% (e.g. McKenzie 1984; Laporte and Watson 1995; Faul 1997). As shown by Hirth and Kohlstedt (1995) and Faul (1997), basaltic melt inclusions in experimentally produced olivine aggregates are surrounded by a combination of curved and flat crystal faces whereby both sets of authors trace the development of flat face to the anisotropy of γ_{SL}. The general striving of mineral grains to minimise their surface energy in a polycrystalline aggregate leads to the development of F-faces, which increase the cross-sectional area of melt-filled channels (Fig. 4) and thus increase the permeability and melt connectivity threshold. This is valid not only for melt-filled triple junctions as shown in Fig. 4 but also for melt pools bound by more than three grains. According to Laporte and Watson (1995), a high anisotropy can result in a decrease in melt connectivity which would reduce permeability due to the increased value of ϕ_C caused by the occurrence of more F-faces. Thus, a high content of minerals with strong anisotropy at very low-melt fractions should result in decreased permeability. At higher degrees of melting, however, high crystal anisotropy acts to maintain high permeability once the melt channels are interconnected.

In applying the order of decreasing anisotropy clinopyroxene > olivine > orthopyroxene > spinel to melt migration in peridotites, it must be remembered that the spinel shows higher wetting angles, and therefore higher surface energies (γ_{SV}) for all crystal faces with respect to the other peridotite minerals (Table 5). Therefore, spinel should have a strong tendency to form F-faces in order to lower its surface energy, causing it to contribute positively to permeability despite its low anisotropy. By contrast, melt channels bound partly by enstatite should exhibit a lower cross-sectional area than those bound by only olivine grains, implying a negative contribution of enstatite to permeability. The reverse should be true for diopside because of its higher anisotropy compared to olivine. Peridotites with high modal clinopyroxene and spinel, and low orthopyroxene contents will therefore tend to have higher permeabilities at moderate- to high-melt fractions, but also higher ϕ_C.

Spinel has the highest surface energies of the minerals treated in this study but generally makes up only between <1 and 5% of the rock. Thus, it will be surrounded principally by olivine in peridotites, as olivine makes up 60–80% of the modal mineralogy (Boyd 1989). The surfaces between spinel and olivine will be characterised by high interfacial energies because of the contrast in surface energies of these two minerals, and so will be preferential sites for melt movement.

Exactly this relationship is seen in samples of dunite from the Inagli intrusion in Siberia, where infiltrating melt surrounds Cr-spinel crystals and Cr-spinel-olivine surfaces are the sites of the first melt infiltration (Zinngrebe 1998). In addition, these spinels frequently show faceted shapes, which corresponds well to the above conclusion concerning the development of F-faces due to the anisotropy of γ_{SL}.

Fertile vs. depleted peridotites

Fertile or metasomatically refertilised peridotite compositions contain higher amounts of clinopyroxene and spinel and lower amounts of orthopyroxene relative to depleted peridotite types (Boyd 1989; Zinngrebe and Foley 1995; McDonough and Rudnick 1998). In terms

of the extractability of melt produced in situ in these fertile peridotite mineral assemblages, a higher degree of melting will be needed before connectivity is achieved. However, once ϕ_C has been surpassed, regions with high modal clinopyroxene and spinel abundances, and low orthopyroxene contents will favour the passage of melts due to the fact that anisotropy can have a positive effect on the permeability only where melt interconnection is already established. Melts from such regions are thus more likely to reach the Earth's surface, so that the chemical signals of mantle metasomatism may be preferentially telescoped into erupting basalts. Furthermore, more fertile bulk compositions should have lower melting temperatures (Falloon and Green 1987), so that the production of sufficient melt to overcome the connectivity threshold will be more common for fertile compositions in the natural environment.

By contrast, orthopyroxene-rich peridotites, which are typical of the subcratonic mantle (Dawson 1980; Boyd 1989), will have low ϕ_C but also low permeabilities once ϕ_C is surpassed. Thus, although lowest-degree partial melts of harzburgites should be more mobile than melts from lherzolites, a higher overall degree of melting must be achieved for effective extraction of large volumes of melt. In addition, the infertile composition of harzburgites makes higher-degree partial melting less likely under realistic geological conditions. The impedance for melt movement caused by high modal orthopyroxene will apply especially to melts with high viscosities, which speaks against the hypothesis that orthoyproxene enrichment in cratonic peridotites may be produced by reaction with silica-rich melts (Rudnick et al. 1994; Kelemen 1995): the first encounter produces orthoyproxene-enriched peridotite which then acts as a barrier to further movement of the silica-rich melt.

The more commonly applicable conclusion from this work is that an orthopyroxene-rich harzburgite will tend to impede the flow-through of melts. This is consistent with the observations of Toramuru and Fujii (1986), according to which the melt phase occurs mainly at triple junctions formed by olivine alone in partially molten olivine aggregates with additional opx and cpx, meaning that the participation of both pyroxenes impedes wetting. This observation, called the "pyroxene effect" by Fujii et al. (1986), can be explained by grain boundaries with comparatively high values of γ_{SS} providing an energetically more favourable pathway for melts than interfaces with lower values, because the melt seeks to reduce the high interfacial energy by wetting. The smallest possible value of γ_{SS} at interfaces of identical minerals with equal orientation is determined solely by the azimuthal misorientation of their lattices, whereas at mixed-mineral interfaces it is a function of the difference in their surface energies (Shelley 1993). Hence, γ_{SS} at interfaces of pyroxenes are likely lower than those for interfaces involving olivine. Statistical evaluations of the dihedral angles performed by Toramuru and Fujii (1986) seem to support this assumption by giving the relations of interfacial energies between the three minerals as follows: $\gamma ol - ol = 1.25 \times \gamma ol - opx = 1.36 \times \gamma ol - cpx$.

Deformed peridotites

The variation in anisotropy of γ_{SL} for the major minerals of spinel peridotites indicates that the segregation and mobility of melts should vary as a function of modal mineral assemblage in undeformed peridotites, and as a function of the degree of deformation in peridotites with similar modal mineral assemblage. Using the results of Toramuru and Fujii (1986), Nakano and Fujii (1989) estimated that the critical modal composition at which melt phase connectivity is obtained is at least 63 vol% olivine for a natural peridotite. In considering the critical melt fraction, Nakano and Fujii (1989) calculated a value of 0.8% for ϕ_C in a peridotite composed of more than 63 vol% olivine. However, despite their usage of polymineralic systems which are closer to natural compositions than purely olivine matrices, the effect of crystal anisotropy on melt distribution and ϕ_C was not taken into account.

For consideration of melt distribution in deformed peridotites the above concept of variable γ_{SS} can be applied. Hydrostatic pressure conditions are probably not a widespread feature within the upper mantle; differential stresses commonly cause deformation and crystallographic alignment of the crystal matrix. Crystal faces with minimum surface energies will be preferably developed perpendicular to the greatest compressible stress (σ_1) whereas faces with higher energy are mostly oriented subparallel to σ_1 (e.g. Bussod and Christie 1991). In the case of a stress field with more or less vertically aligned σ_1, grain boundaries with low interfacial energies should occur perpendicular to σ_1. These low-energy grain boundaries should not easily be wetted by melt, so that a more frequent occurrence of melt along more or less vertically aligned grain boundaries is more likely in deformed regions.

Detailed knowledge of anisotropic surface energies of minerals involved in the generation of primary melts, together with a more complete database on the extent of their anisotropy would be desirable to improve the understanding of extraction and melt modifying processes.

Acknowledgements This research was funded by the Deutsche Forschungsgemeinschaft (DFG; SFB 468). We are grateful for the creative co-operation of workshop members in construction of the experimental apparatus as well as M. Drury for his constructive comments. FNS thanks all his colleagues from Foleys Pub for their help and loyalty.

References

Bischof C, Possart W (1983) Adhäsion, theoretische und experimentelle Grundlagen. Akademie Verlag, Berlin

Boyd FR (1989) Compositional distinction between oceanic and cratonic lithosphere. Earth Planet Sci Lett 96:15–26

Bruno E, Carbonin S, Molin G (1982) Crystal structures of Ca-rich clinopyroxenes on the $CaMgSi_2O_6$-$Mg_2Si_2O_6$ join. Tschermaks Mineral Petrogr Mitteil 29:223–240

Bulau JR, Waff HS (1979) Mechanical and thermodynamic constraints on fluid distribution in partial melts. J Geophys Res 84:6102–6108

Bunge HJ (1985) Representation of preferred orientations. In: Wenk HR (ed) Preferred orientation in deformed metals and rocks; an introduction to modern texture analysis. Academic Press, Orlando, pp 73–108

Bussod GY, Christie JM (1991) Textural development and melt topology in spinel lherzolite experimentally deformed at hypersolidus conditions. J Petrol Spec Lherzolites Issue:17–39

Cmiral M, Fitz Gerald JD, Faul UH, Green DH (1998) A close look at dihedral angles and melt geometry in olivine-basalt aggregates: a TEM study. Contrib Mineral Petrol 130:336–345

Dawson JB (1980) Kimberlites and their xenoliths. Springer, Berlin Heidelberg New York

Drury MR, FitzGerald JD (1996) Grain boundary melt films in an experimentally deformed olivine-orthopyroxene rock: implications for melt distribution in upper mantle rocks. Geophys Res Lett 23:701–704

Falloon TJ, Green DH (1987) Anhydrous partial melting of MORB pyrolite and other peridotite compositions at 10 kbar: implications for the origin of primitive MORB glasses. Mineral Petrol 37:181–219

Faul UH (1997) Permeability of partially molten upper mantle rocks from experiments and percolation theory. J Geophys Res 102:10299–10311

Faul UH, FitzGerald JD (1999) Grain misorientations in partially molten olivin aggregates: an electron backscatter diffraction study. Phys Chem Mineral 26:187–197

Fujii N, Osamura K, Takahashi E (1986) Effect of water saturation on the distribution of partial melt in olivine-pyroxene-plagioclase system. J Geophys Res 91:9253–9259

Hirth G, Kohlstedt DL (1995) Experimental constraints on the dynamics of the partially molten upper mantle: deformation in the diffusion creep regime. J Geophys Res 100:1981–2001

Holness MB (1997) Surface chemical controls on pore-fluid connectivity in texturally equilibrated materials. In: Jamtveit B, Yardley BMD (eds) Fluid flow and transport in rocks. Chapman and Hall, London, pp 149–169

Kelemen PB (1995). Genesis of high-Mg# andesites and the continental crust. Contrib Mineral Petrol 120:1–19

Laporte D, Provost A (1993) Grain-scale distribution of melts in partially molten crustal sources: the importance of anisotropy of solid/liquid interfacial energies on wetting angles. Terra Abstr 5:519

Laporte D, Watson EB (1995) Experimental and theoretical constraints on melt distribution in crustal sources: the effect of crystalline anisotropy on melt interconnectivity. Chem Geol 124:161–184

Levin EM, Robbins CR, McMurdie HF (1974) Phase diagrams for ceramists, 3rd edn. The American Ceramic Society

McDonough WF, Rudnick RL (1998) Mineralogy and composition of the upper mantle. Rev Mineral 37:139–164

McKenzie DP (1984) The generation and compaction of partially molten rock. J Petrol 25:713–765

Nakano T, Fujii N (1989) The multiphase grain control percolation: Its implication for a partially molten rock. J Geophys Res 94:15653–15661

Neumann B (1996) Texturbildende Prozesse in rekristallisierten Quarzpolykristallen. Geotektonische Forsch 87:1–154

Rignault E, Provost A, Laporte D (1996) Modelling the effect of surface energy anisotropy on the grain-scale geometry of a partial melt in a polycrystalline aggregate. Terra Abstr 8:55–56

Rudnick RL, McDonough WF, Orpin A (1994) Northern Tanzanian peridotite xenoliths: a comparison with Kaapvaal peridotites and inferences on metasomatic interactions. In: Meyer OHA, Leonardos OH (eds) Proc 5th Int Kimberlite Conf, Araxa, Brasil, 18 June–4 July 1991. CPRM (Brasilia) Spec Publ 1A, pp 336–353

Scholze H (1988) Glas, Natur, Struktur und Eigenschaften, 3rd edn. Springer, Berlin Heidelberg New York

Shelley D (1993) Igneous and metamorphic rocks under the microscope. Chapman and Hall, London

Toramaru A, Fujii N (1986) Connectivity of melt phase in a partially molten peridotite. J Geophys Res 91:9239–9252

Waff HS, Bulau JR (1979) Equilibrium fluid distribution in an ultramafic partial melt under hydrostatic stress conditions. J Geophys Res 84:6109–6114

Waff HS, Faul UH (1992) Effects of crystalline anisotropy on fluid distribution in ultramafic partial melts. J Geophys Res 97:9003–9014

Wanamaker BJ, Kohlstedt DL (1991) The effect of melt composition on wetting angle between silicate melts and olivine. Phys Chem Mineral 18:26–36

Watson EB, Brenan JM, Baker DR (1990) Distribution of fluids in the continental mantle. In: Menzies MA (ed) Continental mantle. Oxford Monographs 16, pp 111–125

Zinngrebe E (1998) Der Inagli-Dunit (Sibirien): Ein Beispiel für metasomatische Effekte alkaliner Silikatschmelzen in Peridotiten. PhD Thesis, University of Göttingen

Zinngrebe E, Foley SF (1995) Metasomatism in mantle xenoliths from Gees, West Eifel, Germany: evidence for the genesis of calc-alkaline glasses and metasomatic Ca-enrichment. Contrib Mineral Petrol 122:79–96